Superconducting and pseudogap phases from scaling near a Van Hove singularity

J. González
Instituto de Estructura de la Materia, Consejo Superior de Investigaciones Científicas, Serrano 123, 28006 Madrid, Spain
(Received 31 July 2001; revised manuscript received 4 September 2002; published 27 February 2003)

We study the corrections to the Fermi energy induced by the interactions in a two-dimensional electron system, showing that it is attracted towards the Van Hove singularity for a certain range of doping levels. The scaling of the Fermi level allows to cure the infrared singularities left in the BCS channel after renormalization of the leading logarithm near the divergent density of states. A phase of *d*-wave superconductivity arises beyond the point of optimal doping corresponding to the peak of the superconducting instability. For lower doping levels, the condensation of particle-hole pairs due to the nesting of the saddle-points takes over, leading to the opening of a gap for quasiparticles in the neighborhood of the singular points.

DOI: 10.1103/PhysRevB.67.054510 PACS number(s): 74.20.Mn, 71.10.Hf

I. INTRODUCTION

The study of the electronic properties of the cuprates represents nowadays a great challenge from the theoretical point of view, as the phenomenology of these materials has become increasingly rich during the last decade. There have only been a few attempts to develop a theory that may encompass the main experimental features,[1] including the antiferromagnetism of the undoped compounds and the pseudogap phase above the superconducting transition. Additionally, other proposals have focused on the mechanism of superconductivity, stressing the role played by antiferromagnetic fluctuations[2] or by the proximity to a Van Hove singularity (VHS) in the doped materials.[3]

The later approach has received much attention recently, since it establishes a natural competition between magnetic and superconducting instabilities in a two-dimensional (2D) system.[4–8] The investigation of the model of electrons near a VHS is delicate due to the appearance of logarithmic divergences in perturbation theory. In a renormalization group (RG) framework, one has to handle infrared singularities that arise after renormalizing away the leading logarithm, as the energy dependence of some quantities comes in powers of a logarithm square.[9]

Most part of the analyses of the problem have been made fixing the Fermi level at the VHS from the start. This questions the naturalness of the predicted instabilities, that rely critically on the proximity to the singular density of states. The Fermi energy is actually a dynamical quantity that is shifted by interaction effects. It has been shown that the VHS has the tendency to attract the Fermi level of the electron system.[10–14] It is therefore more appropriate to let the chemical potential free to evolve as the states are integrated in the quantum theory. This also solves at once the problem of the infrared divergences, as the shift of the chemical potential from the VHS acts as an infrared cutoff in the logarithmic dependences left in the renormalization.

We illustrate the above ideas in the case of the $t-t'$ Hubbard model, which has a dispersion relation with saddle points at $A=(\pi,0)$ and $B=(0,\pi)$, as depicted in Fig. 1. We consider then a model whose action at the classical level is

$$
\begin{aligned}
S=\sum_a \int d\omega d^2p[\omega\Psi^+_{a\sigma}(\mathbf{p})\Psi_{a\sigma}(\mathbf{p})-(\varepsilon_a(\mathbf{p})\\
-\mu_0)\Psi^+_{a\sigma}(\mathbf{p})\Psi_{a\sigma}(\mathbf{p})]\\
+\sum_{a,b,c,d}\int\prod_{i=1}^{4} d\omega_i d^2p_i U(\mathbf{p}_1,\mathbf{p}_2,\mathbf{p}_3,\mathbf{p}_4)\Psi^+_{a\sigma}(\mathbf{p}_1)\\
\times\Psi^+_{b\sigma'}(\mathbf{p}_2)\Psi_{c\sigma'}(\mathbf{p}_4)\Psi_{d\sigma}(\mathbf{p}_3)\delta(\mathbf{p}_1+\mathbf{p}_2-\mathbf{p}_3-\mathbf{p}_4)\\
\times\delta(\omega_1+\omega_2-\omega_3-\omega_4),
\end{aligned}
$$

where the indices a,b,c,d run over the two patches around A and B, and $\varepsilon_{A,B}(\mathbf{p})\approx\mp(t\mp 2t')p_x^2\pm(t\pm 2t')p_y^2$. The scaling transformation that leaves invariant the kinetic term of the action (at $\mu_0=0$) is

$$\omega\rightarrow s\omega,$$

$$\mathbf{p}\rightarrow s^{1/2}\mathbf{p},$$

$$\Psi_{a\sigma}(\mathbf{p},\omega)\rightarrow s^{-3/2}\Psi_{a\sigma}(\mathbf{p},\omega).$$

It is easily checked that, with the above transformation, the interaction term in the action is also scale invariant for a constant value of the potential $U(\mathbf{p}_1,\mathbf{p}_2,\mathbf{p}_3,\mathbf{p}_4)$. If this is not constant, provided that it is a regular function of the arguments we can resort to an expansion in powers of the mo-

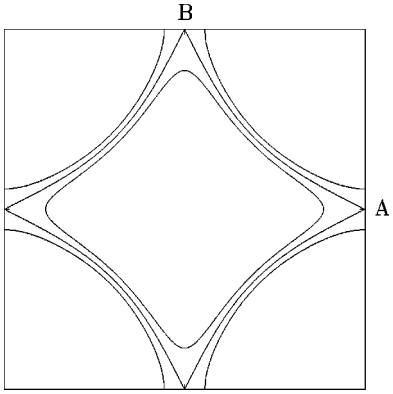

FIG. 1. Contour energy map for the $t-t'$ model about the Van Hove filling.

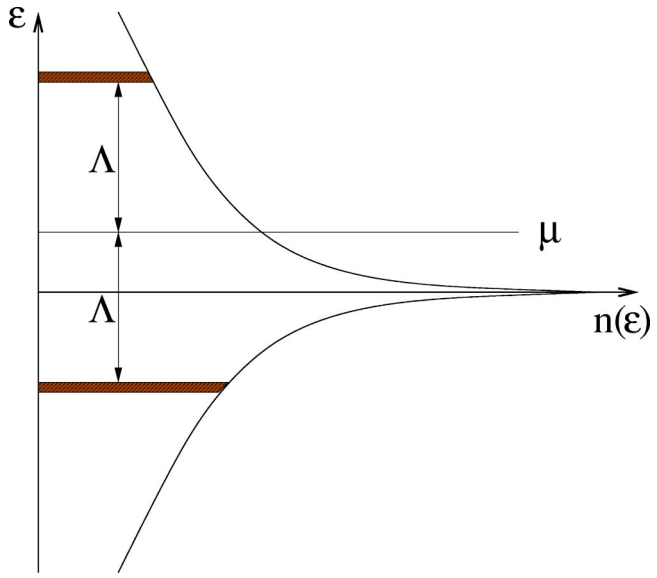

FIG. 2. Picture of the density of states $n(\varepsilon)$ and of the renormalization of the chemical potential μ by integration of states at the energy cutoff Λ.

menta. Only the constant term is significant, since the rest of higher-order terms fade away upon scaling to the low-energy limit $s\rightarrow 0$. Interactions with higher number of fields in the action are also irrelevant in that limit. This means that we meet the first requirement to apply the RG program, that is to have a model that converges to a fixed-point under scaling transformations at the classical level.

We deal with a Wilsonian RG approach in which the chemical potential μ is originally placed away from the VHS, and electron modes in two thin slices about energies $\mu+\Lambda$ and $\mu-\Lambda$ are progressively integrated out, as shown in Fig. 2. This approach assumes that the model is considered at fixed bare chemical potential, so that the statistical description is made in terms of the grand-canonical ensemble. The physical situation corresponds to the case in which the system is in contact with a large reservoir of particles, that fixes the bare value μ_0 of the chemical potential.

An important feature of the Wilsonian approach is that the progressive integration of the high-energy electron modes leads to the reaccomodation of the Fermi level at each RG step, due to the self-energy corrections arising from the charge integrated out. In this computational framework, one adopts the picture in which the chemical potential depends on the energy scale Λ, in the reference frame in which the one-particle levels are held fixed. Then, the renormalized chemical potential $\mu(\Lambda)$ can be thought as a quantity parametrizing the particle number in the system.

In general, in a closed system one does not assign any physical meaning to the bare value of the chemical potential, since it is just set to correspond, after renormalization by the interaction, to a determined number of particles. The situation is different, however, when the model is in contact with a large reservoir of particles. The content of particles in the small system (our 2D system) depends on μ_0 and on the strength with which the particles interact within it. Obviously, a larger repulsion between the particles allows for a larger compensation of the pressure of particles μ_0 exerted by the reservoir. This is the kind of effect that lies in the renormalization of the chemical potential, specially near a VHS where the interaction strength depends implicitly on the density of states.

The renormalization of the chemical potential accounts therefore for the reduction suffered by its effective value in the 2D system due to the repulsive interaction. This computational scheme produces the same results as the equivalent but more physical picture in which, instead of the chemical potential, the one-particle levels are renormalized to higher energies by effect of the repulsive interaction. In this interpretation, the shift of the levels depends again on the amount of charge present in the system, in such a way that the Fermi energy for the renormalized levels is bound to coincide with the nominal chemical potential μ_0 of the reservoir. This picture is dual and completely equivalent to that adopted in our computational framework, in which the chemical potential is seen as renormalized in a system with unrenormalized one-particle levels.

The renormalization of the chemical potential has been already noticed in the general RG analysis of interacting fermion systems.[15] While, in the case of an isotropic dispersion relation, this dependence of $\mu(\Lambda)$ on the cutoff does not have physical significance, the situation is different in the system under consideration since the charge integrated out at each RG step bears the nontrivial dependence of the density of states near the VHS.

The other important difference that introduces the Wilsonian approach with respect to other RG analyses of the model is the significance that acquires the kinematics in the classification of the interaction channels. This has been one of the main remarks made by Shankar in the application of RG techniques to interacting fermion systems.[15] In the simplest version, one reduces the problem to a finite number of couplings corresponding to channels with particular kinematics (the so-called forward-scattering, exchange and BCS channels). This may be considered as a first approximation to capture the behavior of the interaction vertices, which represent a manifold of couplings depending on the momenta of the particles. Some attempts have been already made to incorporate in a more refined way this functional dependence of the interaction within the RG approach.[8]

In what follows, we deal therefore with a RG scheme which is appropriate for the electron system in contact with a charge reservoir, which sets the bare value μ_0 of the ensemble. The evolution of the Fermi level in a model describing the contact of a system near a VHS and a real charge reservoir has been studied in Ref. 14. The results obtained below with the RG approach are in agreement with those of such a detailed analysis. Let us also remark that the consideration of the system at fixed bare chemical potential may be most appropriate for the description of the Cu-O layers of the cuprate superconductors, as these may provide a practical realization of a low-dimensional system (each 2D layer) in contact with a charge reservoir.

II. FERMI LEVEL RENORMALIZATION

The behavior of μ as $\Lambda\rightarrow 0$ can be obtained by solving the Schwinger-Dyson equation $1/G=1/G_0-\Sigma$. The bare

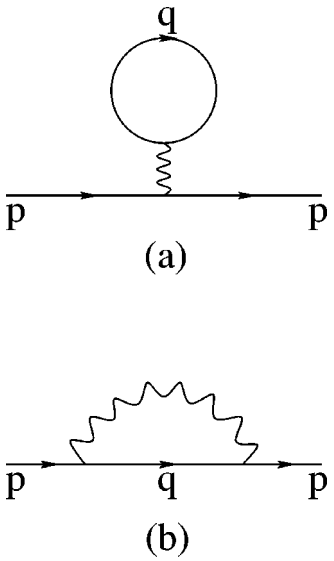

FIG. 3. Diagrams contributing to the electron self-energy at the one-loop level.

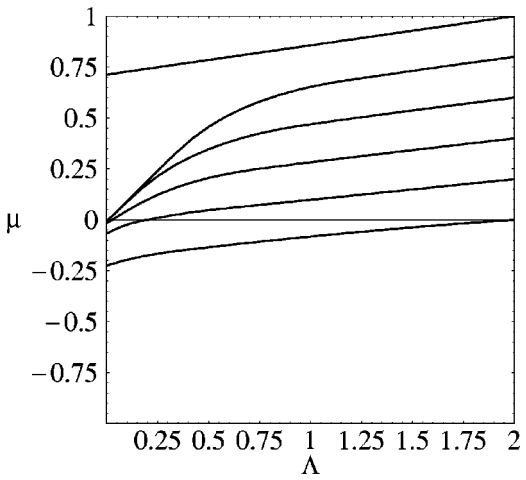

FIG. 4. Scaling of the chemical potential as a function of the high-energy cutoff for a Hubbard coupling $U=4t$. The curves correspond to different values of the bare chemical potential μ_0, given in each case by μ at the highest value of the cutoff.

chemical potential μ_0 in the free propagator G_0 is corrected by the frequency and momentum-independent part of the self-energy Σ. This is given to the one-loop order by the Hartree and exchange diagrams depicted in Fig. 3. At each RG step, the loop integrals are carried over the occupied states in the energy interval $d\Lambda$. The result of this operation is just the charge in the differential slice integrated over, given by $n(\mu-\Lambda)d\Lambda$ in terms of the density of states $n(\varepsilon)$. The differential renormalization of the chemical potential μ becomes then

$$\frac{d\mu}{d\Lambda}=Fn(\mu-\Lambda), \tag{1}$$

where F is the forward-scattering vertex that couples to the charge density.[6]

When extracting the differential correction to the chemical potential, we have neglected terms with derivatives with respect to the cutoff of the quantities at the right-hand-side of Eq. (1), in order to keep the RG equations to the one-loop order. This approximation is actually justified by the fact that the resolution of the one-loop RG equation for the F vertex leads to a weak-coupling regime near the VHS.[6] The cutoff dependence thus obtained for the forward-scattering vertex F has to be taken into account when solving the flow equation (1). We recall that, in terms of the energy scale ε which measures the proximity to the VHS, the F vertex is reduced according to the expression $F(\varepsilon)\approx F_0/[1-cF_0\ln(\varepsilon)/(4\pi^2 t)]$, where $c\equiv 1/\sqrt{1-4(t'/t)^2}$.[6]

The distinctive feature of the VHS is that the density of states $n(\varepsilon)$ diverges logarithmically. As a consequence, the renormalized chemical potential is attracted in a certain range by the VHS as $\Lambda\to 0$. If F were constant, the fixed-point condition $-1+Fn(\tilde{\mu})=0$, with $\tilde{\mu}=\mu-\Lambda$, would give $\mu(\Lambda)$. Taking into account the scaling of the F vertex, it is found that the renormalized value of μ lies very close to the level of the singularity, for appropriate values of the bare chemical potential.

Since the important physical effects take place near the singularity, we may approximate the density of states by the dependence $n(\varepsilon)=zc\ln(t/\varepsilon)/(4\pi^2 t)$ for $|\varepsilon|\leqslant 0.5t$, and constant elsewhere. This has the correct normalization of the logarithmic singularity, including the factor z corresponding to the quasiparticle weight near the VHS. The result of solving the scaling equation (1) for a Hubbard coupling $U=4t$ (with a constant ratio z/t) has been represented in Fig. 4. Similar flow patterns are obtained for a wide range of the interaction strength extending beyond $U=10t$. We observe that there is a range of nominal values of the chemical potential in which this is attracted towards the VHS. As a consequence of that, there is a range of filling levels that are forbidden above the level of the singularity.

We remark that, in the RG approach, the shift of the chemical potential is measured in the reference frame in which the one-particle levels are held fixed. The intuitive physical picture is however the reverse, namely, that the one-particle levels are shifted to higher energy by the repulsive interaction. The shift is proportional to the charge integrated out, until it is reached the point in which the last integrated level coincides with the nominal chemical potential.

An important check is that the reduction of the quasiparticle weight z does not affect the pinning to the VHS displayed by the chemical potential. It is known that the quasiparticles are strongly attenuated due to the enhanced scattering rate near the singularity. This effect appears in the renormalization of the electron self-energy at the two-loop level, where it is seen that both z and the hopping amplitude t are corrected by the interaction. The scaling equations have been obtained in Ref. 12, and they read

$$\Lambda\frac{d}{d\Lambda}\ln z(\Lambda)\approx 6.9\frac{1}{8\pi^4}\frac{U^2}{t^2}, \tag{2}$$

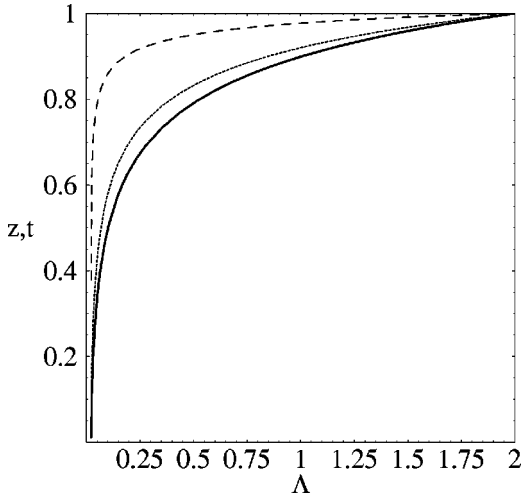

FIG. 5. Curves representing the quasiparticle weight z (solid line), the hopping amplitude t (dotted line), and the ratio z/t (dashed line) as functions of the energy cutoff Λ, for a Hubbard coupling $U=4t$.

$$\Lambda \frac{d}{d\Lambda} \ln t(\Lambda) \approx 5.4 \frac{1}{8\pi^4} \frac{U^2}{t^2}, \tag{3}$$

where U is the bare on-site interaction.[16]

The solution of Eqs. (2) and (3) has been represented in Fig. 5, in units in which $t=1$ at the initial value Λ_0 of the cutoff. We observe that the quasiparticle weight z is renormalized to zero and, at the same time, the hopping amplitude t scales to zero in the low-energy limit. There is however a range, above $\Lambda/\Lambda_0 \approx 0.02$, where the ratio z/t remains of order ~ 1. The pinning of the chemical potential to the VHS shown in Fig. 4 develops above such a value of Λ, which is also below the range of interest for the discussion carried out in the paper. We ensure in this way that the renormalization of the quasiparticle properties does not affect sensibly the scaling of the chemical potential and the determination of the different phases of the model.

We remark again that the correct interpretation of the above results requires the consideration of the system at fixed bare chemical potential, instead of fixed particle number, for each particular RG flow. We reach actually the conclusion that a variation in the bare chemical potential μ_0 does not have always a linear correspondence with the variation of the final renormalized value of μ, which sets the Fermi level of the system. The interplay between the dynamics of the large reservoir that fixes the value of μ_0 and the small system near the Van Hove filling has been studied in Ref. 14. There it has been shown that the system has greater stability when the Fermi level is at the VHS. In that framework, it has been possible to study the evolution of the total energy of the small system and reservoir in terms of the total number of particles, finding that such a function has a local minimum near the Van Hove filling. As an immediate consequence, phase separation takes place in the neighborhood of that filling level, since it is then energetically favorable to have some portion of the system with the Fermi level at the VHS.[14]

It would be of great importance to have the counterpart of the above results in the case of the system considered at fixed particle number. Working in the grand-canonical ensemble, the pinning of the Fermi level to the VHS over a certain range of μ_0 can be realized by exchanging particles with the reservoir. With the system at fixed particle number, however, the situation is unclear. The mechanism of pinning could be realized through the deformation of the Fermi line, as μ_0 varies, to remain closer to the saddle-points of the dispersion relation. This would be consistent with the renormalization of the Fermi line observed in numerical studies of the Hubbard model.[17,18] Such an effect could be also related to the experimental observations reported in Ref. 19. Otherwise, an alternative to achieve the pinning may be the phase separation of the 2D system, with one of the phases at the Van Hove filling and the other at a different filling varying with the doping level. The analysis of which possibility is actually realized is beyond the reach of the methods applied in the present paper. That would require the delicate task of considering the Fermi line as a dynamical object, which may only be afforded at present by discrete numerical approaches of the kind applied in Refs. 5 and 7.

III. RENORMALIZATION OF FOUR-FERMION INTERACTIONS

The scaling of the chemical potential $\mu(\Lambda)$ towards the VHS triggers the different instabilities in the system. These can be traced back to the divergent behavior of some of the interaction channels. The four-point interaction vertex is renormalized at each RG step by a quantity of order $d\Lambda$ when the momentum transfer along a pair of external lines is either $\mathbf{0}$ (forward-scattering channel) or $\mathbf{Q}\equiv(\pi,\pi)$ (exchange channel), or when the total momentum of the incoming modes vanishes (BCS channel). Couplings with less restrictive kinematics can be also included in the Wilsonian RG approach, as it has been done in Ref. 8. It has been shown, however, that the contributions of these couplings to the RG flow are subdominant. The asymptotic behavior of the renormalized couplings is completely determined by the forward-scattering, exchange, and BCS channels. That is, for the purpose of finding the precise divergent behavior of the interaction vertices, the couplings without any of these kinematical restrictions can be safely neglected.[8]

In what follows, we will place in the regime $t' < 0.276t$, in which the forward-scattering interactions are also subdominant. In that range, the divergences at vanishing momentum transfer are related to charge instabilities of the system, which have been treated in detail elsewhere.[14] We will see that divergences in the channel with momentum-transfer $\mathbf{Q}$ give rise to a spin instability, which competes with the superconducting instability in the BCS channel in the model with a bare on-site repulsive interaction.

The different kinematics that may appear in the BCS channel are listed in Fig. 6. We allow for the possibility of Umklapp processes in which the incoming modes scatter from one of the saddle-points to the other.

The different kinematical possibilities that arise in the channel with momentum-transfer $\mathbf{Q}$ are classified in Figs. 7

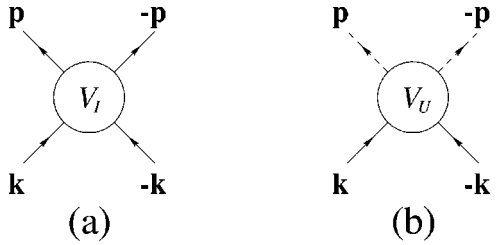

FIG. 6. BCS vertices that undergo renormalization by particle-particle diagrams. The solid and dashed lines stand for modes in the neighborhood of the two different saddle-points.

and 8. The first includes the interactions in which the incoming modes are at different saddle-points, while the latter contains the Umklapp processes. The other important distinction is between direct (D) and exchange (E) processes. Direct processes are those in which the momentum-transfer **Q** is taken by the same scattered fermion line, while in a exchange process the momentum transfer takes place between two different fermion lines connected only by the interaction.

The interaction vertices depicted in Figs. 6–8 are all renormalized upon reduction of the cutoff Λ. This can be traced back to the divergent behavior of the different susceptibilities of the model. By integration of the high-energy modes in the shells of width $d\Lambda$, the particle-hole susceptibility at momentum **Q** gets a contribution

$$d\chi_{ph}(\mathbf{Q}) = \frac{c'}{4\pi^2 t} d\Lambda/\Lambda, \tag{4}$$

where $c' \equiv \ln[(1+\sqrt{1-4(t'/t)^2})/(2t'/t)]$.[20] In the same fashion, the contribution to the particle-particle susceptibility at zero total momentum is

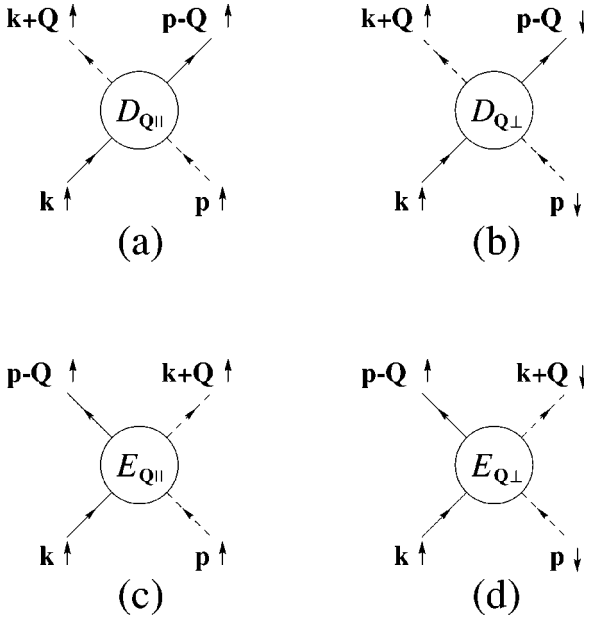

FIG. 7. Direct and exchange vertices that undergo renormalization by particle-hole diagrams.

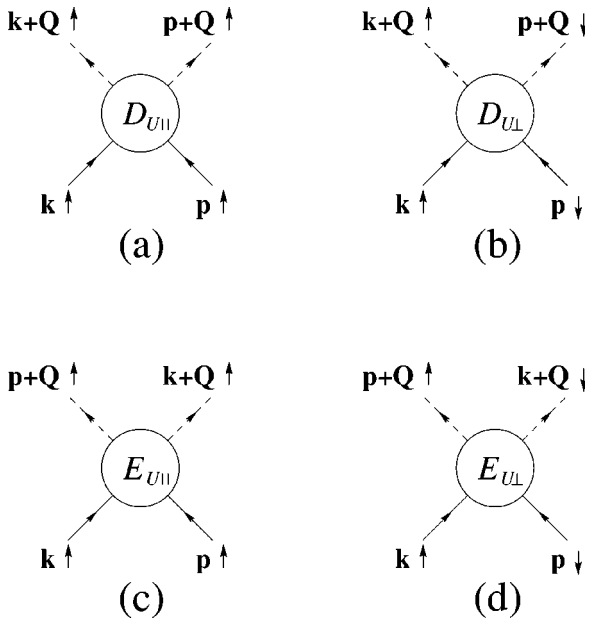

FIG. 8. Umklapp vertices that undergo renormalization by particle-hole diagrams.

$$d\chi_{pp}(\mathbf{0}) = \frac{c}{4\pi^2 t} \ln(\Lambda) d\Lambda/\Lambda. \tag{5}$$

In the latter case, the result of the differential integration diverges logarithmically in the limit $\Lambda \to 0$. This has been a source of problems in the usual RG analyses of the model. The definition of the argument in the logarithm needs an additional scale, while a proper RG scaling requires that the energy is the only dimensionful variable in the problem. It has to be realized that the coefficient at the right-hand-side of Eq. (5) represents actually the density of states. This has to be born in mind for the correct implementation of the RG approach, as we will discuss later.

Let us deal first with the renormalization of the vertices with BCS kinematics in Fig. 6. At the one-loop level, the vertices V_I and V_U get corrections of order $d\Lambda/\Lambda$ from the diagrams shown in Fig. 9. It is important to realize that these are the only diagrams to be taken into account to first order in $d\Lambda$.[15] There are also corrections from particle-hole diagrams but, as long as the momentum that goes into the particle-hole loop is not precisely zero or **Q**, these terms are of order $(d\Lambda)^2$ and therefore irrelevant in the low-energy limit, as shown graphically in Fig. 10.

The BCS vertices mix between themselves alone at the one-loop level, and the situation is similar in that respect to the general analysis of the 2D Fermi liquid.[15] The degree of renormalization depends on the density of states $n(\varepsilon)$ at the shells integrated out. For later use, we consider at this point the most general case in which the chemical potential μ does not coincide from the start with the level of the VHS. The differential RG equations take then the form

$$\Lambda \frac{\partial V_I}{\partial \Lambda} = cn(\mu - \Lambda)(V_I^2 + V_U^2), \tag{6}$$

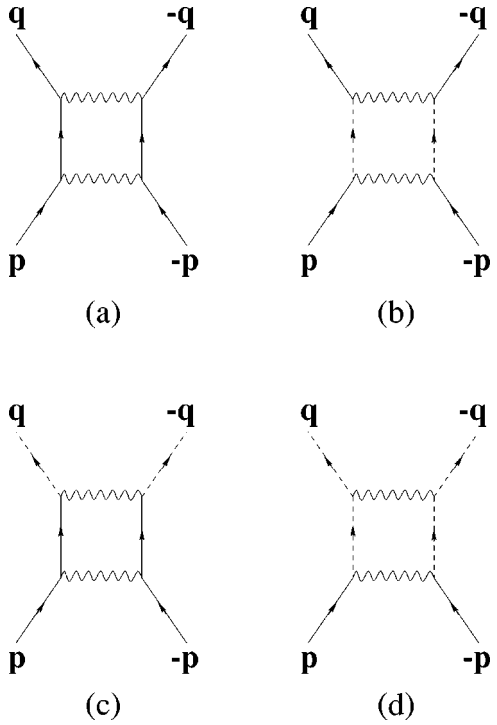

FIG. 9. Particle-particle diagrams renormalizing the BCS vertices at the one-loop level.

$$\Lambda \frac{\partial V_U}{\partial \Lambda} = 2cn(\mu - \Lambda) V_I V_U . \tag{7}$$

These equations were considered in Ref. 4, and they also appear at the dominant level in the RG approach of Ref. 8.

We consider next the renormalization of the vertices $E_{\mathbf{Q}\perp}$ and $E_{U\perp}$, which have also the property that they mix only between themselves in the one-loop corrections linear in $d\Lambda$. These have been represented in Fig. 11. It can be checked that any other diagrams give irrelevant contributions of order $(d\Lambda)^2$, because they involve either a particle-hole susceptibility at momentum different from $\mathbf{Q}$ or a particle-particle susceptibility with total momentum different from zero. In the latter case, for instance, it is shown in Fig. 12 that the number of intermediate states produced by integration of high-energy modes is quadratic, instead of linear in $d\Lambda$.

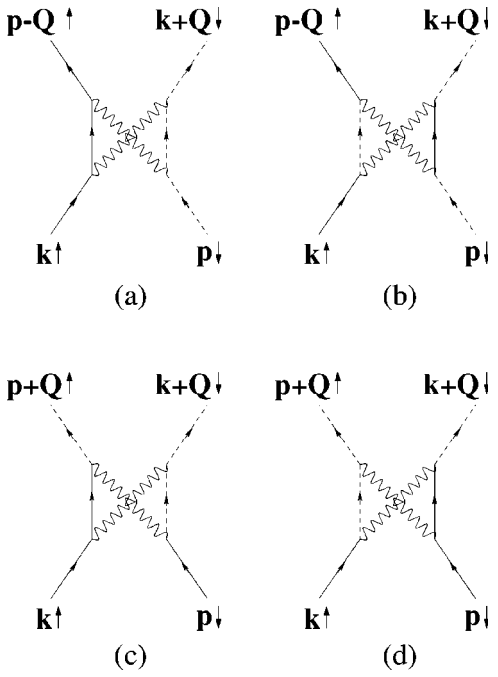

FIG. 11. Particle-hole diagrams renormalizing the vertices $E_{\mathbf{Q}\perp}$ and $E_{U\perp}$ at the one-loop level.

The differential RG equations for the pair of vertices read

$$\Lambda \frac{\partial E_{\mathbf{Q}\perp}}{\partial \Lambda} = -c'(E_{\mathbf{Q}\perp}^2 + E_{U\perp}^2)/(4\pi^2 t), \tag{8}$$

$$\Lambda \frac{\partial E_{U\perp}}{\partial \Lambda} = -c' E_{\mathbf{Q}\perp} E_{U\perp}/(2\pi^2 t). \tag{9}$$

These equations were obtained in Ref. 4, where the names U_{inter} and U_{umk} were used instead of $E_{\mathbf{Q}\perp}$ and $E_{U\perp}$ introduced in the present paper. The same equations also arise at the dominant level in the functional renormalization of Ref. 8.

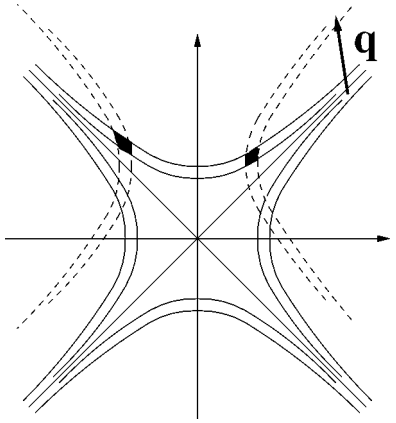

FIG. 10. Picture of the high-energy shells of width $d\Lambda$ at a given saddle point. The dark regions represent the contribution to a particle-hole diagram when $\mathbf{q}$ is the total incoming momentum.

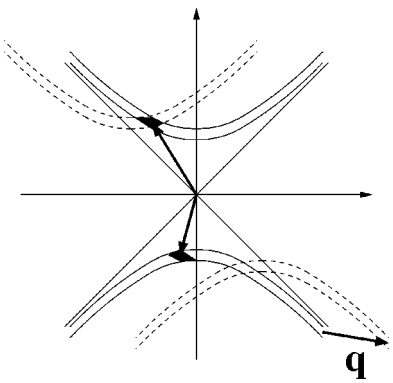

FIG. 12. Same scheme as in Fig. 10. The dark regions represent the contribution to a particle-particle diagram when $\mathbf{q}$ is the total incoming momentum.

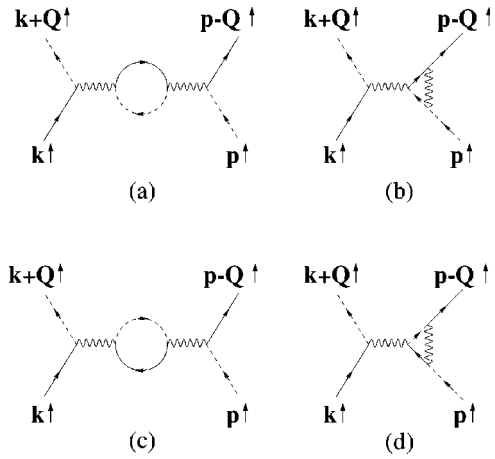

FIG. 13. Particle-hole diagrams renormalizing the vertex $D_{\mathbf{Q}\parallel}$ at the one-loop level.

We now turn to the rest of the vertices, $D_{\mathbf{Q}\parallel}$, $D_{\mathbf{Q}\perp}$, $E_{\mathbf{Q}\parallel}$, $D_{U\parallel}$, $D_{U\perp}$, and $E_{U\parallel}$, which renormalize among themselves at the one-loop level. It is clear that the vertices $D_{\mathbf{Q}\parallel}$ and $E_{\mathbf{Q}\parallel}$ cannot be distinguished from each other just by looking at the external legs. The same applies to $D_{U\parallel}$ and $E_{U\parallel}$. At the one-loop level, one can still discern whether the momentum-transfer $\mathbf{Q}$ takes place along the same scattered fermion line or not. However, the different corrections have to organize so that the above pairs of vertices enter in the combinations $D_{\mathbf{Q}\parallel}-E_{\mathbf{Q}\parallel}$ and $D_{U\parallel}-E_{U\parallel}$, which are the quantities that make physical sense. In that respect, the situation is similar to what happens with the couplings $g_{1\parallel}$ and $g_{2\parallel}$ in the one-dimensional electron systems.[21]

The one-loop renormalization of the vertices provides an explicit proof of the above statement. The vertex $D_{\mathbf{Q}\parallel}$ gets linear corrections in $d\Lambda$ from the diagrams shown in Fig. 13, while $E_{\mathbf{Q}\parallel}$ is renormalized by the diagrams shown in Fig. 14. Their RG equations read then

$$\Lambda\frac{\partial D_{\mathbf{Q}\parallel}}{\partial\Lambda}=c'(D_{\mathbf{Q}\parallel}^2+D_{\mathbf{Q}\perp}^2+D_{U\parallel}^2+D_{U\perp}^2-2D_{\mathbf{Q}\parallel}E_{\mathbf{Q}\parallel}-2D_{U\parallel}E_{U\parallel})/(4\pi^2t), \tag{10}$$

$$\Lambda\frac{\partial E_{\mathbf{Q}\parallel}}{\partial\Lambda}=-c'(E_{\mathbf{Q}\parallel}^2+E_{U\parallel}^2)/(4\pi^2t). \tag{11}$$

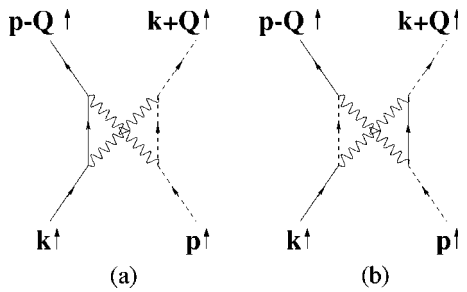

FIG. 14. Particle-hole diagrams renormalizing the vertex $E_{\mathbf{Q}\parallel}$ at the one-loop level.

These two equations can be combined to be written in terms of the physical vertex,

$$\Lambda\frac{\partial(D_{\mathbf{Q}\parallel}-E_{\mathbf{Q}\parallel})}{\partial\Lambda}=c'[(D_{\mathbf{Q}\parallel}-E_{\mathbf{Q}\parallel})^2+(D_{U\parallel}-E_{U\parallel})^2+D_{\mathbf{Q}\perp}^2+D_{U\perp}^2]/(4\pi^2t). \tag{12}$$

The RG equation for $D_{\mathbf{Q}\perp}$ also depends on the combinations $D_{\mathbf{Q}\parallel}-E_{\mathbf{Q}\parallel}$ and $D_{U\parallel}-E_{U\parallel}$, since we have

$$\Lambda\frac{\partial D_{\mathbf{Q}\perp}}{\partial\Lambda}=c'[(D_{\mathbf{Q}\parallel}-E_{\mathbf{Q}\parallel})D_{\mathbf{Q}\perp}+(D_{U\parallel}-E_{U\parallel})D_{U\perp}]/(2\pi^2t) \tag{13}$$

As a final check, the equations for $D_{U\parallel}-E_{U\parallel}$ and $D_{U\perp}$ turn out to depend on the physical combination of couplings

$$\Lambda\frac{\partial(D_{U\parallel}-E_{U\parallel})}{\partial\Lambda}=c'[(D_{\mathbf{Q}\parallel}-E_{\mathbf{Q}\parallel})(D_{U\parallel}-E_{U\parallel})+D_{\mathbf{Q}\perp}D_{U\perp}]/(2\pi^2t), \tag{14}$$

$$\Lambda\frac{\partial D_{U\perp}}{\partial\Lambda}=c'[(D_{\mathbf{Q}\parallel}-E_{\mathbf{Q}\parallel})D_{U\perp}+(D_{U\parallel}-E_{U\parallel})D_{\mathbf{Q}\perp}]/(2\pi^2t). \tag{15}$$

As long as the above RG equations depend explicitly on the spin projection, they allow to see how the spin-rotational invariance can be preserved along the RG orbits. For this purpose one has to look at the response functions for the spin operator, checking the conditions under which they become independent of the spin direction. An analysis of this kind has been carried out in Ref. 14 considering the uniform magnetization of the system. Since we are dealing with renormalized interactions at large momentum-transfer $\mathbf{Q}=(\pi,\pi)$, we focus now on the correlations of the Fourier transform of the spin operator at that momentum transfer, $S_j(\mathbf{Q})$, with $j=x,y,z$.

We pay attention to the frequency dependence of the spin response functions, which can be established through their scaling properties.[22] The response function $R_z(\omega)$ for the $S_z(\mathbf{Q})$ operator, for instance, is renormalized by the diagrams shown in Fig. 15. After taking the derivative with respect to the cutoff and imposing the self-consistency of the diagrammatic expansion, we obtain

$$\Lambda\frac{\partial R_z}{\partial\Lambda}=-\frac{2c'}{\pi^2t}+\frac{c'}{\pi^2t}(D_{\mathbf{Q}\parallel}-E_{\mathbf{Q}\parallel}+D_{U\parallel}-E_{U\parallel}-D_{\mathbf{Q}\perp}-D_{U\perp})R_z. \tag{16}$$

The response functions $R_x(\omega)$ and $R_y(\omega)$ for the other two components of the spin operator are both renormalized by the diagrams shown in Fig. 16. Following the same procedure as for $R_z(\omega)$, we obtain

$$\Lambda\frac{\partial R_x}{\partial\Lambda}=-\frac{2c'}{\pi^2t}-\frac{c'}{\pi^2t}(E_{\mathbf{Q}\perp}+E_{U\perp})R_x \tag{17}$$

and a completely similar equation for $R_y(\omega)$.

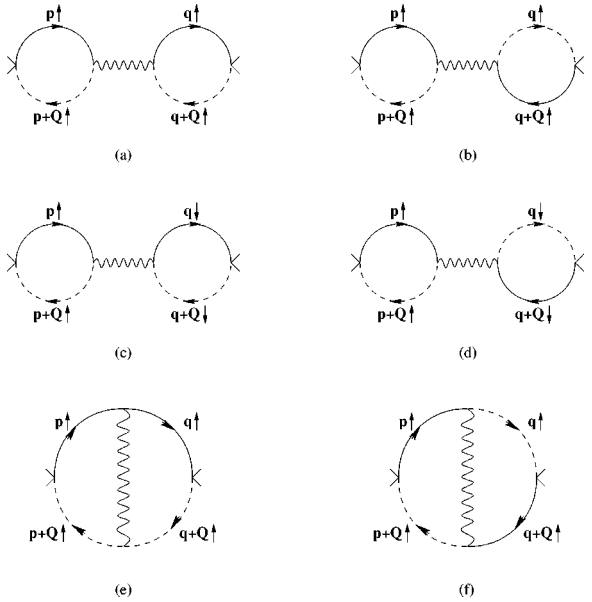

FIG. 15. First-order contributions to the correlator of the S_z operator.

The response functions $R_x(\omega)$, $R_y(\omega)$, and $R_z(\omega)$ can be made exactly equal if the equation

$$D_{\mathbf{Q}\parallel}-E_{\mathbf{Q}\parallel}+D_{U\parallel}-E_{U\parallel}-D_{\mathbf{Q}\perp}-D_{U\perp}=-E_{\mathbf{Q}\perp}-E_{U\perp} \tag{18}$$

is satisfied all along the flow. From Eqs. (8), (9), (12)–(15), we observe that this is automatically fulfilled when the condition is imposed for the initial values of the couplings. In the case of the Hubbard model, for instance, we have before the renormalization of the couplings

$$D_{\mathbf{Q}\perp}+D_{U\perp}-D_{\mathbf{Q}\parallel}+E_{\mathbf{Q}\parallel}-D_{U\parallel}+E_{U\parallel}=E_{\mathbf{Q}\perp}+E_{U\perp}=2U. \tag{19}$$

The condition (18) is actually satisfied by the bare couplings of any Hamiltonian that is invariant under rotations. We show in this way that, in the Wilsonian RG approach, the SU(2) spin symmetry can be preserved at each point of the RG flow of the couplings.

The RG equations that we have obtained can be considered as a first step towards a functional renormalization of the interaction vertices. These depend on the momenta of the incoming and outgoing particles, and it is natural that they may be renormalized with different strength under different regimes of the momenta. We have taken into account the channels that develop the strongest divergences in the Wilsonian RG approach. Restricting the analysis to the forward-scattering, the exchange and the BCS kinematics, the renormalization program can be carried out self-consistently with a reduced number of couplings.

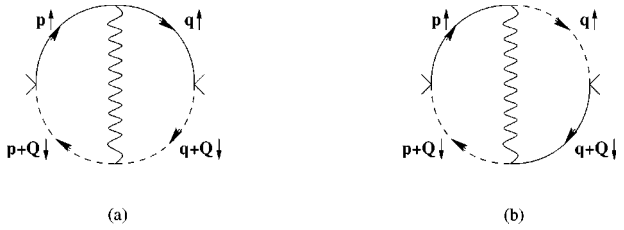

FIG. 16. First-order contributions to the correlators of the S_x and S_y operators.

In Ref. 8, a scheme has been proposed to go beyond the consideration of the channels with special kinematics, by assigning a number of generic couplings to the interaction vertices when the momenta of the particles do not fall within the restrictive conditions. Although the RG equations of the couplings for the special kinematics get corrections from the generic couplings, it turns out that the asymptotic behavior of the solutions is completely determined by the former set. The couplings called g_2^x and g_3^x in Ref. 8 correspond precisely to our couplings $E_{\mathbf{Q}}$ and E_U, while those called there g_3^{BCS} and g_4^{BCS} correspond to our definitions for V_U and V_I, respectively. At the dominant level, that is keeping the dominant terms which give the divergent asymptotic behavior, the RG equations of Ref. 8 for the mentioned couplings coincide with our Eqs. (6)–(9). The rest of our RG equations provide the extension to the more involved situation in which the couplings depend explicitly on the spin projection.

Certainly, a more satisfactory RG approach should try to keep some form of continuity in the momentum dependence of the renormalized vertices. Between the couplings for the special kinematics and those which apply to generic distributions of the momenta, there should be incorporated the intermediate instances which may still develop some degree of divergence. It is not likely that the most refined RG equations may lead to different results regarding the dominant divergences obtained at the present stage, but a true functional renormalization would provide the definitive check that the divergences in the interaction vertices develop for localized distributions of the momenta, specially in what concerns those with the highest critical scale.

IV. SPIN AND SUPERCONDUCTING INSTABILITIES

If one were to take the bare coupling U of the Hubbard model as the initial point of the RG scaling, the set of Eqs. (6) and (7) would not provide interesting physics. This is so because we would have in such case $V_I=V_U=U$, and sending the cutoff to zero would simply reduce monotonically the interactions in these channels. However, the diagonals in this space of couplings mark the boundary between the regions of stable and unstable scaling. The slightest perturbation with $V_I<V_U$ will make the couplings to grow large, pointing at the appearance of new features in the system.

An interesting effect comes from the fact that, even in the Hubbard model, there are corrections that vanish in the low-energy limit $\Lambda\to 0$ (irrelevant operators) but may drive to the unstable regime at the early stages of the scaling. The Kohn-Luttinger effect, that leads to a pairing instability in the Fermi liquid at very low energies,[23] can be established on the same grounds in the RG framework.[15] In the case of the Hubbard model, the corrections to V_I and V_U are given by the horizontal iteration of the bubble diagrams in Fig. 17. The momentum flowing to the bubbles is not in general close to **0**, in the first case, nor to **Q**, in the second. In the Wilso-

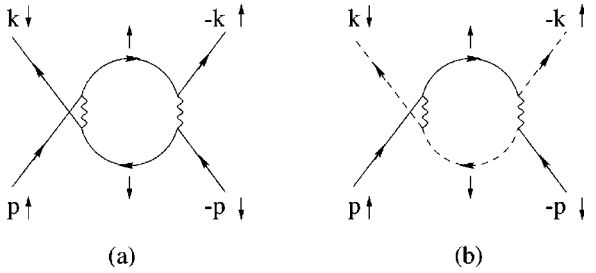

FIG. 17. Particle-hole corrections to the BCS vertices in the Hubbard model.

nian RG scheme, these particle-hole bubbles scale therefore as $\sim(d\Lambda)^2$, and they are considered irrelevant contributions.[15]

In the Hubbard model with $t'<0.276t$, the corrections coming from the iteration of diagram (a) in Fig. 17 have smaller strength than those from diagram (b).[4] As long as these are antiscreening diagrams, i.e., they add to the bare repulsive interaction, the conditions are met to have an unstable scaling for the vertices in Fig. 6, with the above constraint on t and t'. The singular behavior develops for the combination V_I-V_U, in which the particle-particle diagrams build up a pole for an imaginary value of the frequency. The physical interpretation is that there is a condensation of Cooper pairs at the scale where the vertex function diverges.[24] The symmetry of the order parameter turns out to be *d*-wave, as the combination V_I-V_U corresponds to having opposite amplitudes in the two saddle-points.

In our approach, the scaling of the chemical potential $\mu(\Lambda)$ allows to deal with a finite density of states in Eqs. (6) and (7) during the RG flow. The result of computing the scale at which V_I-V_U diverges, for a value of the Hubbard coupling $U=4t$ and $t'=0.16t$, has been represented in Fig. 18. A singularity is only found for values of the bare chemical potential $\mu_0=\mu(\Lambda_0)$ that lead to attraction of the Fermi level to the VHS. The curve of the critical scale reaches a maximum for a certain value of optimal doping, and then it decreases for smaller values of μ_0 as the chemical potential is not precisely pinned to the VHS in the low-energy limit.

The instability in the BCS channel has to be matched against the strong tendency towards a magnetic instability at wave-vector $\mathbf{Q}=(\pi,\pi)$ for $t'<0.276t$.[4] In the RG framework, this comes from the divergent behavior of the solutions of Eqs. (8), (9), (12)–(15), in the case of the Hubbard model with $U>0$. As shown in the preceding section, the spin-rotational invariance is preserved along the RG orbits. We can therefore carry out the analysis of the solutions for a given choice of the spin projection, in particular for the $E_{\mathbf{Q}\perp}+E_{U\perp}$ channel that governs the correlations of the S_x and S_y operators. In the low-energy limit, a singularity in the couplings is reached at a certain value of Λ. The important point is that the logarithmically divergent particle-hole bubbles building up the singularity have an imaginary part equal to $i\pi/2$ times $c'/(4\pi^2 t)$, which means that the vertex gets actually a pole for an imaginary value of the frequency.

Thus, the divergence in this channel gives rise to the condensation of particle-hole pairs with momentum $\mathbf{Q}$. This physical interpretation is similar to that of the superconducting instability,[24] but the presence in this case of a macroscopic number of particle-hole pairs leads to nonvanishing expectation values of the type $U\int d^3k\langle\Psi^+_{A\uparrow}(\mathbf{k})\Psi_{B\downarrow}(\mathbf{k}+\mathbf{Q})\rangle \equiv\Delta$, $\Psi_{\alpha\sigma}(\mathbf{k})$ being the electron field operator at saddle-point α. This has a drastic effect in the low-energy spectrum, since the electron propagator is corrected by the insertion of the condensate as shown in Fig. 19. The result is that a gap of magnitude $|\Delta|$ opens up in the spectrum of quasiparticles. The appearance of this gap takes place in the neighborhood of the saddle-points. It can be shown that the size of the Fermi line destroyed by the nesting of such points is $\lesssim\sqrt{|\Delta|/t'}$, in units of the inverse lattice spacing.

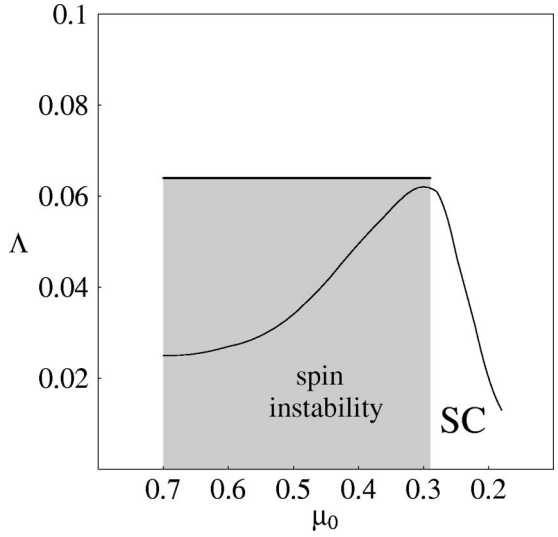

FIG. 18. Plot of the energy scale of the superconducting instability (thin line) and of the transition to the phase with spin instability (thick line). This phase is given by the shaded region in the diagram, while the region to its right and below the thin line corresponds to the phase where the superconducting correlations prevail.

The point at which the vertex $E_{\mathbf{Q}\perp}+E_{U\perp}$ diverges can be estimated from Eqs. (8) and (9), and it has been represented in Fig. 18 for our particular choice $t'=0.16t$. The scale of condensation of particle-hole pairs is larger than the scale of the superconducting instability up to the point of optimal doping marked by the peak of the latter. In our computational framework, the energy scale of the former instability has a constant behavior as a function of the bare chemical potential μ_0. This is due to the fact that, in the absence of a precise knowledge of the renormalization of the complete Fermi line, we can only discern that the particle-hole corrections diverge whenever the Fermi level remains pinned to the VHS. In the range of values of μ_0 displayed in Fig. 18 down to $\mu_0\approx0.29$, the final renormalized values of the chemical

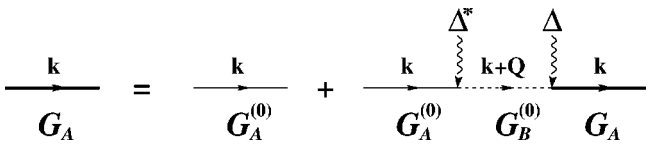

FIG. 19. Self-consistent equation for the dressed electron propagator G in the particle-hole condensate, in terms of the undressed propagators $G_A^{(0)}$ and $G_B^{(0)}$ at the two inequivalent saddle-points.

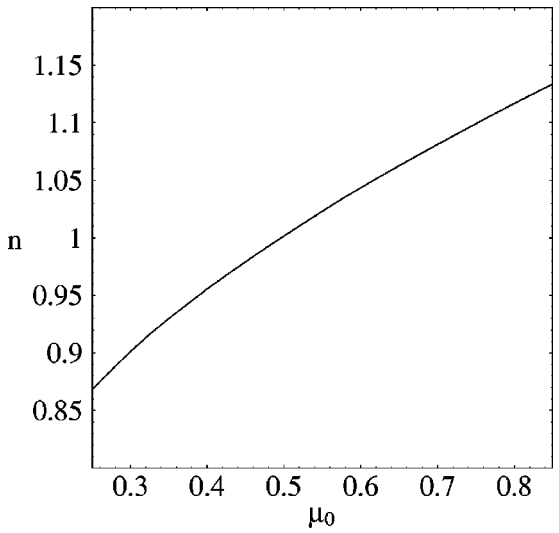

FIG. 20. Plot of the correspondence between μ_0 (measured with respect to the level of the VHS) and the band filling n, obtained from a constant renormalization of the bare chemical potential as discussed in the text.

potential lie very close to the level of the VHS, as observed in Fig. 4. Then we may assume, as a first approximation, that the scaling towards the magnetic instability is equally strong over that range of μ_0. This assumption breaks down when the renormalized chemical potential departs from the VHS by an amount comparable to the own gap that would arise from the instability. When this happens, it can be assured that the scaling is arrested before the singularity in the magnetic response function is reached. This marks the boundary of the magnetic phase at $\mu_0 \approx 0.29$.

In a more accurate description of a real system, it is conceivable that the energy scale giving the onset of the magnetic instability may have a smooth dependence on the doping level. This may arise from the renormalization of the t' parameter in the process of pinning of the Fermi level. That analysis requires however the knowledge of the dynamics of the whole Fermi surface, and it goes beyond the present computational framework.

At this point, it may be convenient to establish a relation between the values of μ_0 and the band fillings resulting in the case that the system were closed instead of being in contact with the charge reservoir fixing the value of μ_0. To draw a continuous correspondence, we have determined the band filling given by the Fermi level that would be obtained from μ_0 upon a conventional renormalization due to the interaction (as in the upper and the lower curve of Fig. 4). The results are represented in Fig. 20, where n stands for the band filling of the 2D system.

For low doping levels, the opening of a gap of magnitude $|\Delta|$ is the effect that prevails, and the renormalization of the interactions is stopped at that energy scale. On the other hand, the superconducting instability takes over beyond the optimal doping. This point corresponds to the situation where the chemical potential remains closer to the VHS during its RG flow while, at the same time, the deviation of the final renormalized value already becomes of the same order that the gap opening up in the spectrum. As mentioned before, the scaling of $E_{\mathbf{Q}\perp}+E_{U\perp}$ relies on the pinning to the VHS and, beyond the optimal doping, it is therefore arrested before the singularity in the vertex is reached. This is in contrast to the scaling in the BCS channel, which is given by Eqs. (6) and (7) irrespective of the pinning to the VHS.[15] The strength of the superconducting instability is however modulated by the proximity to the VHS, and it fades away as the final value of the renormalized chemical potential departs sensibly from the level of the singularity.

The divergence in the $E_{\mathbf{Q}\perp}+E_{U\perp}$ channel may result in a nonvanishing expectation value with spin projection S_x or S_y, depending on the choice of the condensate wave function. A similar divergence in the channel with momentum-transfer $\mathbf{Q}$ and no spin-flip shows that $U\int d^3k\langle \Psi^+_{A\uparrow}(\mathbf{k})\Psi_{B\uparrow}(\mathbf{k}+\mathbf{Q})\rangle$ has also an absolute value precisely equal to $|\Delta|$. Depending on the different combinations of phases, the spin of the condensate may point in any direction of the space, providing another manifestation of the rotational invariance of the Wilsonian RG scheme.

When considering the model strictly at zero temperature, the ground state of the system is forced to choose a definite projection of the spin. The condensation of particle-hole pairs leads then to the spontaneous breakdown of the SO(3) invariance. As a consequence, a pair of Goldstone bosons arise corresponding to spin waves on top of the condensate of particle-hole pairs. In the regime below optimal doping where the magnetic instability prevails, these are the gapless excitations of the spectrum together with the quasiparticles from the regions not affected by the nesting of the saddle-points.

We have thus clarified the nature of the magnetic instability that arises when the Fermi level is pinned to the VHS of the electron system. The main physical effect is the condensation of particle-hole pairs, which results in the opening of a gap for the quasiparticles in the neighborhood of the saddle-points. This is the dominant instability up to the optimal doping marked by the peak of the scale of the superconducting instability, which takes over for higher doping levels.

The properties that we have discussed rely on the existence of an attractive fixed-point in the scaling of the chemical potential of the 2D system. They are therefore robust as they do not depend on fine-tuning or on the particular details of the model, what may explain some of the universal properties of the hole-doped copper-oxide superconductors. As it has been emphasized, the correct interpretation of the RG results implies actually the consideration of the 2D system in contact with a charge reservoir which fixes the bare chemical potential. From a conceptual point of view, it would be very important to understand the mechanism of pinning of the Fermi level in a closed system. This may require the development of new techniques, able to incorporate the whole dynamical evolution of the Fermi line in the renormalization process, which is not afforded by the present computational schemes.

ACKNOWLEDGMENTS

Fruitful discussions with F. Guinea are gratefully acknowledged. This work has been partly supported by CICyT (Spain) and CAM (Madrid, Spain) through Grants Nos. PB96/0875 and 07N/0045/98.

[1] See, for instance, E. Dagotto, Rev. Mod. Phys. **66**, 763 (1994); and P.W. Anderson, *The Theory of Superconductivity in the High-T_c Cuprates* (Princeton Univ., Princeton, 1997).
[2] N.E. Bickers, D.J. Scalapino, and S.R. White, Phys. Rev. Lett. **62**, 961 (1989); P. Monthoux, A.V. Balatsky, and D. Pines, Phys. Rev. B **46**, 14 803 (1992).
[3] D.M. Newns, H.R. Krishnamurthy, P.C. Pattnaik, C.C. Tsuei, and C.L. Kane, Phys. Rev. Lett. **69**, 1264 (1992); P.C. Pattnaik, C.L. Kane, D.M. Newns, and C.C. Tsuei, Phys. Rev. B **45**, 5714 (1992); L.B. Ioffe and A.J. Millis, *ibid.* **54**, 3645 (1996); for a review, see R.S. Markiewicz, J. Phys. Chem. Solids **58**, 1179 (1997).
[4] J.V. Alvarez, J. González, F. Guinea, and M.A.H. Vozmediano, J. Phys. Soc. Jpn. **67**, 1868 (1998).
[5] C.J. Halboth and W. Metzner, Phys. Rev. B **61**, 7364 (2000); Phys. Rev. Lett. **85**, 5162 (2000).
[6] J. González, F. Guinea, and M.A.H. Vozmediano, Phys. Rev. Lett. **84**, 4930 (2000).
[7] C. Honerkamp, M. Salmhofer, N. Furukawa, and T.M. Rice, Phys. Rev. B **63**, 035109 (2001).
[8] B. Binz, D. Baeriswyl, and B. Douçot, Eur. Phys. J. B **25**, 69 (2002).
[9] H.J. Schulz, Europhys. Lett. **4**, 609 (1987); I.E. Dzyaloshinskii, Sov. Phys. JETP **66**, 848 (1987).
[10] R.S. Markiewicz, J. Phys.: Condens. Matter **2**, 665 (1990).
[11] J. González, F. Guinea, and M.A.H. Vozmediano, Europhys. Lett. **34**, 711 (1996).
[12] J. González, F. Guinea, and M.A.H. Vozmediano, Nucl. Phys. B **485**, 694 (1997).
[13] G. Kastrinakis, Physica C **340**, 119 (2000).
[14] J. González, Phys. Rev. B **63**, 045114 (2001).
[15] R. Shankar, Rev. Mod. Phys. **66**, 129 (1994).
[16] It has been shown in Ref. 12 that the Lorentz-like symmetry of the $t(k_x^2-k_y^2)$ saddle-point dispersion is preserved by the interaction, so that the main renormalization of the saddle-point band is encoded in the parameters z and t.
[17] D. Duffy and A. Moreo, Phys. Rev. B **52**, 15 607 (1995).
[18] A. Himeda and M. Ogata, Phys. Rev. Lett. **85**, 4345 (2000).
[19] A.A. Kordyuk, S.V. Borisenko, M.S. Golden, S. Legner, K.A. Nenkov, M. Knupfer, J. Fink, H. Berger, L. Forró, and R. Follath, Phys. Rev. B **66**, 014502 (2002). It has been shown there that the Fermi line of Bi-2212 bends progressively as the doping level is increased, in such a way that even in the overdoped regime it does not lose its hole-like character.
[20] H.Q. Lin and J.E. Hirsch, Phys. Rev. B **35**, 3359 (1987).
[21] J. Sólyom, Adv. Phys. **28**, 201 (1979).
[22] H.J. Schulz, in *Correlated Electron Systems*, edited by V. J. Emery (World Scientific, Singapore, 1993), Vol. 9.
[23] W. Kohn and J.M. Luttinger, Phys. Rev. Lett. **15**, 524 (1965).
[24] A.A. Abrikosov, L.P. Gorkov, and I.E. Dzyaloshinski, *Methods of Quantum Field Theory in Statistical Physics* (Dover, New York, 1975), Chap. 7.